MOLECULAR AND CELLULAR BIOLOGY, Dec. 2009, p. 6380–6390 Vol. 29, No. 24
0270-7306/09/$12.00 doi:10.1128/MCB.00116-09

MST Kinases Monitor Actin Cytoskeletal Integrity and Signal via c-Jun N-Terminal Kinase Stress-Activated Kinase To Regulate $p21^{Waf1/Cip1}$ Stability[▽]

Ruth M. Densham,† Eric O'Neill,‡ June Munro, Ireen König, Kurt Anderson, Walter Kolch, and Michael F. Olson*

The Beatson Institute for Cancer Research, Garscube Estate, Switchback Road, Glasgow G61 1BD, United Kingdom

Received 26 January 2009/Returned for modification 9 March 2009/Accepted 30 September 2009

As well as providing a structural framework, the actin cytoskeleton plays integral roles in cell death, survival, and proliferation. The disruption of the actin cytoskeleton results in the activation of the c-Jun N-terminal kinase (JNK) stress-activated protein kinase (SAPK) pathway; however, the sensor of actin integrity that couples to the JNK pathway has not been characterized in mammalian cells. We now report that the mammalian Ste20-like (MST) kinases mediate the activation of the JNK pathway in response to the disruption of the actin cytoskeleton. One consequence of actin disruption is the JNK-mediated stabilization of $p21^{Waf1/Cip1}$ (p21) via the phosphorylation of Thr57. The expression of MST1 or MST2 was sufficient to stabilize p21 in a JNK- and Thr57-dependent manner, while the stabilization of p21 by actin disruption required MST activity. These data indicate that, in addition to being components of the Salvador-Warts-Hippo tumor suppressor network and binding partners of c-Raf and the RASSF1A tumor suppressor, MST kinases serve to monitor cytoskeletal integrity and couple via the JNK SAPK pathway to the regulation of a key cell cycle regulatory protein.

The actin cytoskeleton is a dynamic structure that determines cell morphology and motility. In addition, the cytoskeleton also influences other biological functions, such as proliferation, survival, and death, although the mechanistic details linking the cytoskeleton to these processes have not been fully elucidated. Considerable effort has focused on characterizing the signal transduction pathways that control cytoskeletal organization (33). The actin cytoskeleton itself also may regulate cell signaling; for example, mechanical stretching, shear stress, and cytoskeletal disruption each have been shown to activate stress-activated protein kinase (SAPK) pathways (34). Although in *Saccharomyces cerevisiae* an actin integrity-responsive pathway has been identified in which actin cytoskeleton disassembly results in the activation of the Ssk2p kinase that lies upstream of the Hog1 SAPK pathway (7, 56), an analogous pathway in mammalian cells has not been delineated.

SAPK pathways are specific examples of mitogen-activated protein kinase (MAPK) cascades (43). At the bottom of archetypal MAPK pathways are signal-propagating kinases such as ERK1 and ERK2; in the case of SAPK signaling, the similarly positioned kinases are JNK and p38 family members. MAPK are phosphorylated and regulated by MAPK kinases (MAP2K); for c-Jun N-terminal kinase (JNK), the MAP2K are MKK4 and MKK7, while for p38 they are MKK3 and MKK6. Moving stepwise further upstream are MAP3K and MAP4K, although in some pathways there may be no need for a MAP4K, the Ras activation of the MAP3K Raf in the ERK MAPK pathway being one example.

Although much recent interest has focused on their antiproliferative and proapoptotic functions as a component of the Salvador-Warts-Hippo tumor suppressor network (31) and as binding partners of the c-Raf MAP3K (42) and RASSF1A tumor suppressor (39), the mammalian Ste20-like kinases 1 and 2 (MST1 and MST2, respectively) were first identified (17) because of their homology with the *Saccharomyces cerevisiae* Ste20 MAP4K that acts upstream of three MAPK cascades, including the Ste11/Pbs2/Hog1 SAPK pathway (51). Although the MST kinase domains are very similar to those in Ste20 and mammalian p21-activated kinases (PAK), there is little homology outside this domain, and as a result MST1 and MST2 make up their own Ste20 subfamily without direct orthologues prior to the emergence of the bilaterian subregnum. Given the homology with Ste20, initial characterization focused on the possibility that MST kinases were involved in MAPK regulation, and indeed MST kinases were found to activate SAPK pathways (27), which was associated with the activation of MKK6 and MKK7 (27). It also was found that MST1 coexpression with a kinase-dead version of the MAP3K MEKK1 blocked JNK activation (26). Consistently with these results, MST1 could not activate JNK in cells deleted for both MAP2K enzymes MKK4 and MKK7 (53). Therefore, it appears that MST kinases work at the same level (MAP4K) as Ste20 in the regulation of the SAPK pathways. Although proapoptotic signaling has been shown to contribute to MST activation via

* Corresponding author. Mailing address: The Beatson Institute for Cancer Research, Garscube Estate, Switchback Road, Glasgow G61 1BD, United Kingdom. Phone: 44 (0)141 330 3654. Fax: 44 (0)141 942 6521. E-mail: m.olson@beatson.gla.ac.uk.

† Present address: Cancer Genetics Laboratory, Department of Medical & Molecular Genetics, King's College Medical School, Guy's Hospital, Tower Wing, Great Maze Pond, London SE1 9RT, United Kingdom.

‡ Present address: Radiation Oncology and Biology, University of Oxford, Old Road Campus Research Building, Churchill Hospital, Oxford OX3 7DQ, United Kingdom.

▽ Published ahead of print on 12 October 2009.

caspase-mediated proteolysis, which removes an autoinhibitory domain (27), little is known about how other nonapoptotic stimuli regulate MST.

There are several possible consequences resulting from the activation of SAPK pathways in response to modifications to actin cytoskeleton organization or integrity. Actin disruption and consequent JNK activation may induce cell cycle arrest (23) or apoptosis (11), or it may promote cell survival (2). We previously showed that one way JNK activation following cytoskeletal disruption might contribute to cell cycle arrest is through the stabilization of the cyclin-dependent kinase inhibitor (CDKI) $p21^{Waf1/Cip1}$ (p21) (14). The eventual outcome of SAPK activation following actin cytoskeleton modification may be influenced by signal intensity, duration, and cellular context. Further progress toward determining how cytoskeletal disruption generates these outcomes will be possible when the details describing how actin cytoskeletal changes activate SAPK signaling have been established.

We wished to determine whether MST kinases sense the integrity of the actin cytoskeleton and link with SAPK signaling. We found that MST2 was colocalized with filamentous actin structures. The expression of MST1 or MST2 was sufficient to activate JNK1, and cytoskeletal disruption activated MST as well as JNK1 in an MST-dependent manner. One consequence of actin disruption is the JNK-mediated stabilization of p21, which was determined to be via phosphorylation of Thr57. The expression of MST1 or MST2 was sufficient to stabilize p21 in a JNK- and Thr57-dependent manner, while the stabilization of p21 by actin disruption required MST activity. These data indicate that MST kinases serve to monitor cytoskeletal integrity and couple via the JNK SAPK pathway to the regulation of a key cell cycle regulatory protein.

MATERIALS AND METHODS

Cell culture. NIH 3T3 mouse fibroblasts and HeLa cervical carcinoma cells were grown at 5% CO_2 in Dulbecco's modified Eagle's medium (DMEM; GibcoBRL) supplemented with penicillin and streptomycin and either 10% (vol/vol) donor calf serum (NIH 3T3; GibcoBRL) or fetal calf serum (HeLa; Harlan). Transient transfections were performed with Lipofectamine 2000 (Invitrogen). Cells were grown routinely in 6-cm dishes to 70% confluence. Plasmid DNA (0.5 μg) was incubated in 30 μl phosphate-buffered saline (PBS) plus 4 μl Lipofectamine 2000 for 20 min before addition to 2 ml serum-free DMEM and incubation on cells for 5 h. Cells were restimulated with 10% donor calf serum overnight (~16 h).

Western blotting. Western blotting was performed as previously described (15). The following primary antibodies were used: Krs1/2 (MST2; C-19), RhoA (26C4), β-actin (C-4), JNK1 (C-17), p21 (C-19-G), and β-tubulin (D10) were from Santa Cruz; JNK1/2 (56G8), phospho-c-Jun (Ser63), c-Jun, and MST1 were from Cell Signaling; MST2-N-term was from Epitomics; FLAG-M2 was from Sigma; and ERK2 was a gift from Chris Marshall (ICR, London, United Kingdom). Alexa-Fluor680 (Molecular Probes)- or IRDye800 (Rockland)-conjugated secondary antibodies were detected and quantified by direct scanning using a Li-Cor Odyssey.

Immunofluorescence. Cells were fixed and stained for immunofluorescence as described previously (16). In brief, cells were grown on coverslips and treated as described before being fixed in 4% paraformaldehyde in PBS for 15 min. Coverslips were washed twice with PBS and then permeabilized by incubation with 0.5% Triton X-100–PBS for 10 min, washed three times with 1% bovine serum albumin (BSA)–PBS before incubation with FLAG-M2 (1:1,000; Sigma) for 1 h at room temperature, and washed three times with 1% BSA–PBS before incubation with anti-mouse antibody–fluorescein isothiocyanate (1:1,000) and/or Texas red phalloidin (0.5 μg/ml) for 1 h at room temperature, and finally, coverslips were washed three times with 1% BSA–PBS and twice with distilled water before being mounted on slides with Prolong Gold mounting medium. Confocal images were obtained using an Olympus FV1000 confocal microscope using a 60× oil immersion objective.

For total internal reflection fluorescence (TIRF) microscopy, cells were grown in 3-cm glass-bottomed dishes (Iwaki), fixed, and stained as described above. Cells were stored in PBS containing β-mercaptoethanol as an antifade and were sealed with parafilm.

TIRF. TIRF experiments were performed using a Nikon Eclipse TE 2000-U microscope equipped with 60× and 100× (1.45 numerical aperture) Nikon TIRF oil immersion objectives. The Nikon epifluorescence condenser was replaced with a custom condenser in which laser light was introduced into the illumination pathway directly from the optical fiber output oriented parallel to the optical axis of the microscope. The light source for evanescent wave illumination was a 473-nm diode laser or a 561-nm laser (Omicron), with each laser line coupled into the condenser separately to allow individual TIRF angle adjustments. The lasers were controlled by a DAC 2000 card or a Uniblitz shutter operated by MetaMorph (Molecular Devices). A green/red dual filter block (ET-GFP/mcherry from AHF Analysentechnik, Germany) was used for dual-color 473- and 561-nm excitation. A Multi-Spec dual emission splitter (Optical Insights, NM) with a 595-nm dichroic and two bandpass filters (510 to 565 nm for green and 605 to 655 nm for red) was used to separate both emissions. All imaging was performed with a Cascade 512F EMCCD camera (Photometrics, United Kingdom).

Protein stability analysis. NIH 3T3 cells were transfected as indicated and grown in serum-free medium for 16 h prior to treatment with the protein synthesis inhibitor emetine (20 μM) and combinations of Tat-C3 (0.5 μM), latrunculin B (LTB) (200 nM), cytochalasin D (CTD) (200 nM), and SP600125 (30 μM) as indicated for 2 h. Whole-cell lysates were probed for p21 and ERK2 and quantified by infrared imaging as described above.

Immunoprecipitation assays. Cells were grown to 80% confluence in 10-cm dishes, transfected, and/or treated as specified. Cells were washed quickly in ice-cold PBS, lysed in 200 μl of ice-cold TG lysis buffer (20 mM Tris-HCl, pH 8; 140 mM NaCl; 1 mM EGTA; 1% Triton X-100; 10% glycerol; 1.5 mM $MgCl_2$; 1 mM sodium vanadate; 1 mM phenylmethylsulfonyl fluoride; 20 μM leupeptin; 50 mM sodium fluoride), and centrifuged (14,000 × *g* for 10 min at 4°C), and the protein concentration was determined using a bicinchoninic acid protein assay kit (Pierce). Normalized lysates were immunoprecipitated by incubation with 30 μl protein A Sepharose plus antibody for Krs1/2 (MST2) or JNK1 (C-17) for 2 to 3 h with rotation at 4°C. Beads were washed three times in ice-cold buffer (50 mM Tris, pH 7.5; 200 mM NaCl; 0.1% Triton X-100) before resuspension in Laemmli buffer and analysis by sodium dodecyl sulfate-polyacrylamide gel electrophoresis (SDS-PAGE).

In-gel and immunoprecipitation kinase assays. In-gel kinase assays of MST1/2 activity were performed as follows: SDS–12% PAGE gels were poured that contained 0.5 mg/ml myelin basic protein (MBP) as a protein substrate. Samples were run as described for Western blotting, and then the gels were washed sequentially to remove SDS, denature, and renature the proteins as follows: three 20-min washes in 20% propanol, 50 mM Tris, pH 8; three 20-min washes in 50 mM Tris, pH 8, 5 mM β-mercaptoethanol; one 60-min wash in 6 M guanidine-HCl, 50 mM Tris, pH 8, 5 mM β-mercaptoethanol; three 20-min washes and then overnight incubation in 50 mM Tris, pH 8, 5 mM β-mercaptoethanol, 4% Tween 20 at 4°C; finally, the gel was reequilibrated to room temperature in a 30-min wash of 40 mM HEPES, pH 8, 10 mM $MgCl_2$, 2 mM dithiothreitol (DTT). The kinase assay was performed by the incubation of the gel with 40 mM HEPES, pH 8, 10 mM $MgCl_2$, 0.5 mM EGTA, 50 μM ATP, 25 μCi [γ-^{32}P]ATP for 2 h at room temperature before the reaction was stopped by washing the gel approximately 10 times in 5% trichloroacetic acid, 1% sodium pyrophosphate. Finally, the gel was dried and analyzed using a phosphorimager.

For JNK immunoprecipitation/kinase assays, JNK immunoprecipitations were carried out as described above, but with a final wash in SAPK buffer (20 mM HEPES, pH 7.5, 20 mM β-glycerophosphate, 10 mM $MgCl_2$, 1 mM DTT, 50 μM sodium vanadate). Beads were resuspended in 30 μl SAPK buffer containing 2.5 μg glutathione *S*-transferase (GST)-c–Jun 1-79, 10 μM ATP, and 2.5 μCi [γ-^{32}P]ATP. Kinase reactions were carried out at 30°C for 30 min with shaking and terminated by the addition of 10 μl 4× Laemmli sample buffer. Samples were resolved by SDS-PAGE; gels were fixed, stained with Coomassie, and dried before analysis by phosphorimaging.

For the recombinant JNK phosphorylation of GST–c-Jun, FLAG-p21, or FLAG-T57A, FLAG-p21 and FLAG-T57A were transiently expressed in HEK293 cells and purified by precipitation using FLAG-agarose beads (Sigma). Recombinant GST–c-Jun was expressed and purified as described previously (40). Beads were washed stringently three times with 50 mM Tris, pH 7.5, 500 mM NaCl, 0.1% Triton X-100, followed by three washes with 50 mM Tris, pH 7.5, 200 mM NaCl, 0.1% Triton X-100. JNK kinase assays were performed on the

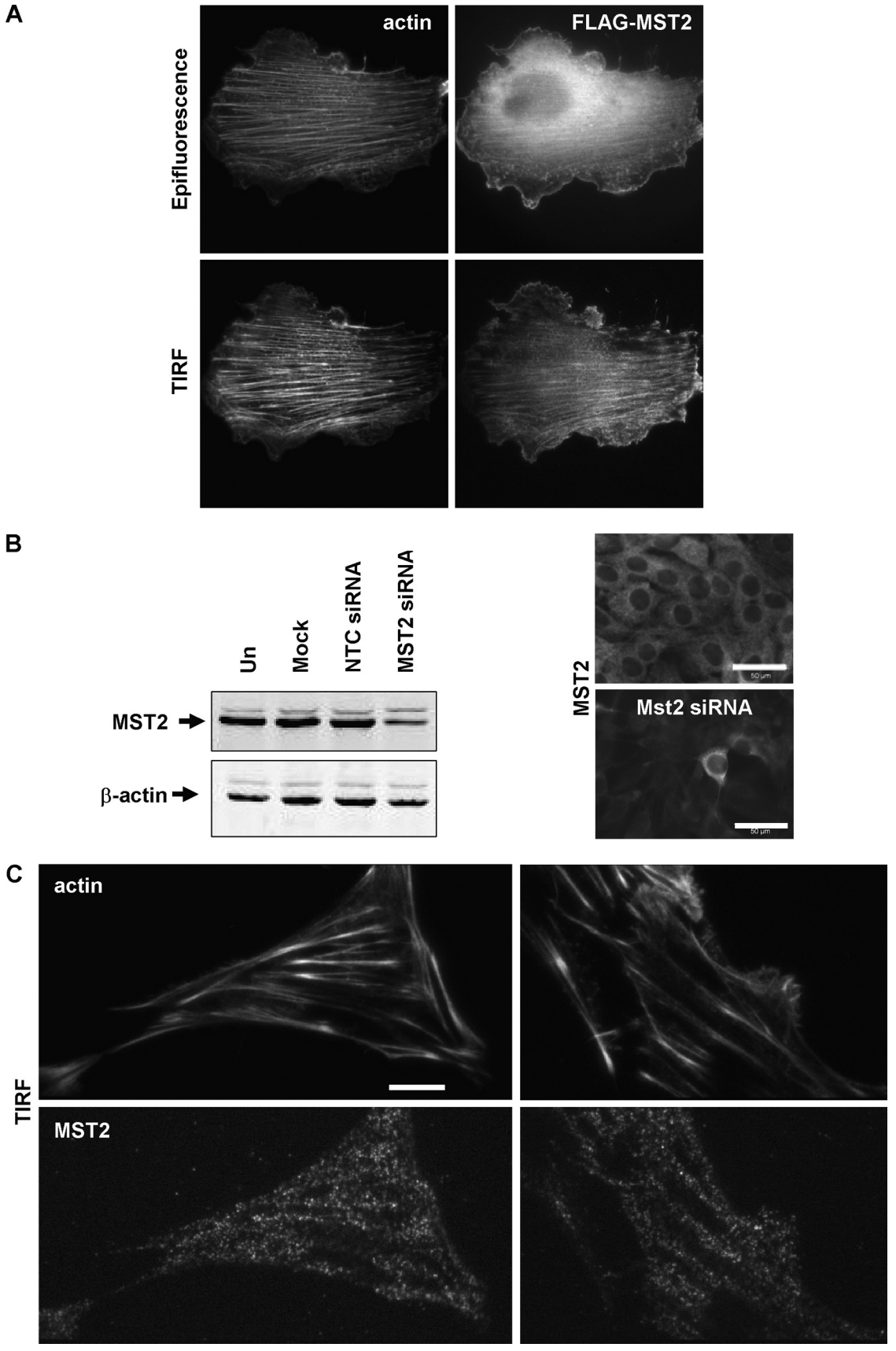
A
actin
FLAG-MST2
Epifluorescence
TIRF
B
Un
Mock
NTC siRNA
MST2 siRNA
MST2
β-actin
MST2
Mst2 siRNA
C
actin
TIRF
MST2

purified proteins with 0.2 μl recombinant JNK2a (Upstate/Millipore) in SAPK buffer containing 10 μM ATP and 2.5 μCi [γ-^{32}P]ATP as described above.

Mutagenesis. The site-directed mutagenesis of FLAG-p21 was carried out using the QuikChange site-directed mutagenesis kit (Stratagene) according to the manufacturer's protocol. The following PCR oligonucleotides designed to incorporate T57A, S98A, S130A, T145A, and S146A mutations were used: T57A, 5′-CTTTGTCACCGAGGCGCCACTGGAGGGTG-3′ (forward) and 5′-CAC CCTCCAGTGGCGCCTCGGTGACAAAG-3′ (reverse); S98A, 5′-CGGCCTG GCACCGCGCCTGCTCTGCTG-3′ (forward) and 5′-CAGCAGAGCAGGCG CGGTGCCAGGCCG-3′ (reverse); S130A, 5′-CAGGCTGAAGGGGCCCCA GGTGGACCTG-3′ (forward) and 5′-CAGGTCCACCTGGGGCCCCTTCAGC CTG-3′ (reverse); T145A, 5′-GAAACCGGCGGCAGGCTAGCATGACAG-3′ (forward) and 5′-CTGTCATGCTAGCCTGCCGCCGGTTTC-3′ (reverse); and S146A, 5′-CGGCGGCAGACCGCGATGACAGATTTC-3′ (forward) and reverse 5′-GAAATCTGTCATCGCGGTCTGCCGCCG-3′ (reverse).

RNAi. For RNA interference (RNAi), NIH 3T3 or HeLa cells were seeded at 1 to 1.5 × 10^5 cells/well in 6-well dishes and grown overnight and then were transfected with On-Target Plus Smartpool (Dharmacon) short interfering RNA (siRNA) against mouse MST2 (STK3; L-040440-00), human MST2 (STK3; J-J 004874-07), or a nontargeting control (NTC; D-001810-01). siRNA was mixed with 200 μl Optimem (Gibco) containing 4 μl Lipofectamine 2000 (Invitrogen) per well and incubated at room temperature for 20 min. Cells were grown in 2 ml Optimem, and 200 μl of siRNA master mix was added dropwise to each well. After 6 h, donor calf serum (DCS) was added to a final concentration of 10%. Twenty-four hours after transfection, the medium was changed to Dulbecco's modified Eagle's medium containing 10% DCS supplemented with penicillin and streptomycin, and cells were grown for a further 48 h before treatment and lysis.

RESULTS

Cytoskeleton-associated MST kinases are activated by actin disruption. Although previous studies found that MST1 was predominantly cytoplasmic and could translocate to the nucleus when phosphorylated (36) or caspase cleaved (36), a more precise characterization of MST subcellular localization has not been reported. To examine subcellular localization, we expressed FLAG epitope-tagged MST2 in NIH 3T3 cells and found that the distribution appeared to be largely diffuse in the cytoplasm and excluded from the nucleus, with a degree of filamentous actin (F-actin) colocalization (Fig. 1A). We then used TIRF microscopy to evaluate MST2 localization adjacent to the cell-substrate interface, which is highly enriched for F-actin structures (21). Compared to the more diffuse cytoplasmic localization observed using standard epifluorescence (Fig. 1A, upper), the TIRF image revealed a more distinct pattern that was coincident with the F-actin staining observed using phalloidin (Fig. 1A, lower). There was no appreciable effect of either MST1 or MST2 on F-actin organization (data not shown). To examine the distribution of endogenous MST, we first screened commercial MST antibodies that, following the siRNA-mediated knockdown of MST1 or MST2 (Fig. 1B, left), would display reduced staining by immunofluorescence (Fig. 1B, right). The apparently greater MST2 knockdown by immunofluorescence likely reflects the lower sensitivity of this method. Only one suitable antibody for MST2 was identified in this way, and none were identified for MST1. Endogenous MST2 staining was similar to that of the transfected FLAG-MST2, with a largely cytoplasmic distribution that was excluded from nuclei and some organization in filamentous structures (Fig. 1B). We again used TIRF microscopy to evaluate MST2 localization adjacent to the F-actin-enriched cell-substrate interface, and we found a strikingly similar pattern of distribution of MST2 and F-actin (Fig. 1C). These results suggest that a proportion of MST2 is associated with the actin cytoskeleton.

We next wished to determine whether disrupting actin structures affected MST kinase activity. Initially, F-actin disruption was achieved by inhibiting Rho activity with a cell-permeable Tat fusion form of the *Clostridium botulinum* C3 exoenzyme (45), which inactivates Rho by ADP-ribosylation at asparagine 41 (3). We took advantage of the ability of immunoprecipitated MST2 to renature following polyacrylamide gel electrophoresis in order to perform in-gel kinase assays using MBP as the substrate (17, 52). As shown in Fig. 2A, although comparable levels of MST2 were immunoprecipitated, kinase activity was significantly higher following Tat-C3 treatment. To directly disrupt the actin cytoskeleton, cells were treated with one of two commonly used F-actin-destabilizing drugs: CTD (from *Zygusporium mansonii*), which caps F-actin and stimulates G-actin ATP hydrolysis (47), or LTB (from *Latrunculia magnificans*), which binds G-actin monomers and blocks polymerization into filaments (50). As shown in Fig. 2B, CTD, LTB, and Tat-C3 each significantly disrupted actin structures, although the final cell morphologies were not identical. To decrease experimental variability by reducing the number of sample-handling steps and to increase the throughput of the kinase assays, we performed in-gel MST kinase assays on whole-cell extracts from each condition. Following F-actin disruption, there was increased MBP activity observed at the same 57-kDa molecular mass as that observed for the immunoprecipitated MST2 (Fig. 2C). The identities of the significantly higher-molecular-mass MBP-phosphorylating proteins are unknown. In each case, there was no apparent change in MST1 or MST2 levels (Fig. 2C), nor was there the appearance of lower-molecular-mass caspase-cleaved MST forms (27 and data not shown).

Previous studies showed that MST acted as a MAP4K upstream of the JNK SAPK pathway (27). The disruption of actin

FIG. 1. MST2 colocalizes with F-actin. (A) NIH 3T3 cells transfected with plasmid encoding FLAG epitope-tagged MST2 were fixed and stained with anti-FLAG antibody and Texas red phalloidin to visualize F-actin structures. TIRF microscopy was used to examine MST2 distribution proximal to the cell-substrate interface. While epifluorescence (EPI) microscopy showed that the MST2 distribution was a mixture of diffuse and organized, TIRF revealed that the MST2 distribution was strikingly similar to that of the actin filaments observed at the region of the cell that is enriched for these cytoskeletal structures. Scale bar = 10 μm. (B) To validate antibodies for immunofluorescence, MST2 was knocked down with siRNA in NIH 3T3 cells (left). MST2 levels were comparable in untransfected (Un), mock-transfected, or nontargeting control (NTC)-transfected cells, but the levels were reduced in cells transfected with MST2 siRNA. Untransfected (upper right) and MST2 siRNA-transfected (lower right) cells were stained with anti-MST2 antibody and analyzed by immunofluorescence. MST2 knockdown detected by Western blotting also was observed by immunofluorescence with one commercial antibody. Scale bars = 50 μm. (C) NIH 3T3 cells were fixed and stained with anti-MST2 antibody and Texas red phalloidin to visualize F-actin structures. TIRF microscopy was used to examine MST2 distribution proximal to the cell-substrate interface; two examples are shown. As with transfected MST2, TIRF revealed that the endogenous MST2 distribution was similar to that of the actin filaments observed at the region of the cell that is enriched for these cytoskeletal structures. Scale bar = 10 μm.

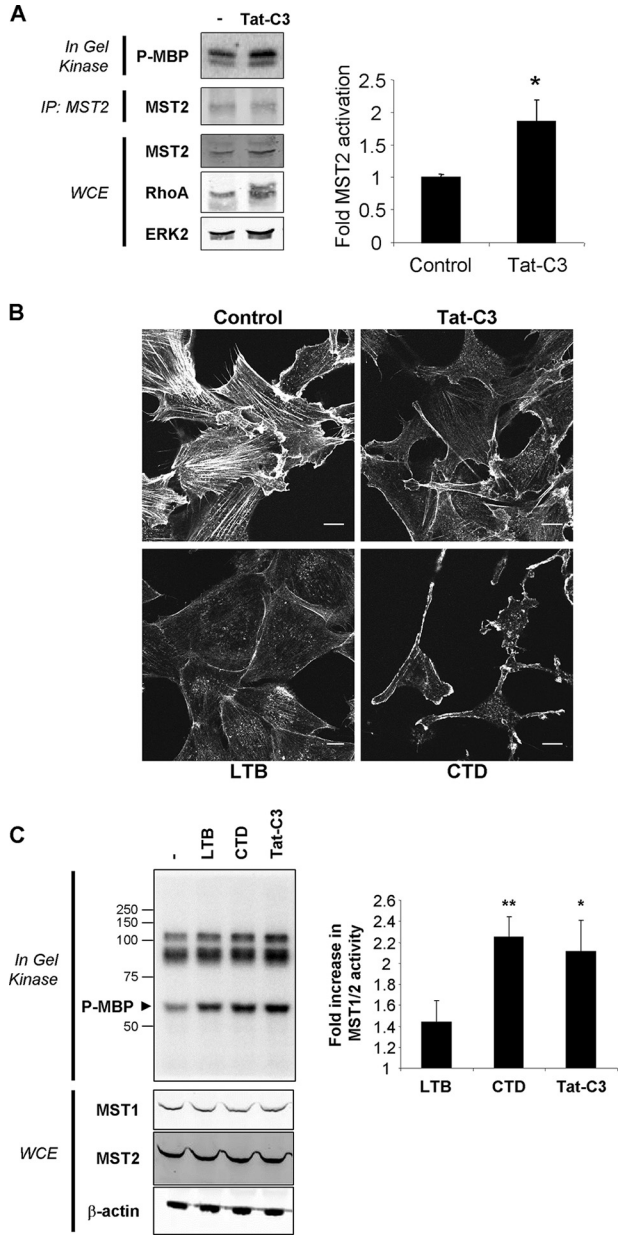

FIG. 2. Actin cytoskeleton disruption activates MST kinases. (A) MST2 immunoprecipitated from NIH 3T3 cells treated with cell-permeable TAT-C3 exoenzyme (0.5 μM) had significantly increased activity compared to that from untreated control cells using an in-gel kinase assay (*, $P < 0.05$ by Student's t test; data are means ± standard errors of the means; $n = 3$). The lower band in the kinase assay likely represents immunoprecipitated (IP) MST1 due to the cross-reactivity of the antibody. The blotting of whole-cell extracts (WCE) showed equivalent levels of MST2 and ERK2 in each condition. Treatment with Tat-C3 produced a characteristic change in the mobility of a proportion of RhoA. (B) Disruption of the actin cytoskeleton in NIH 3T3 fibroblasts with CTD (200 nM), LTB (200 nM), or Tat-C3 (0.5 μM). Cells were fixed and stained with Texas red phalloidin to visualize F-actin structures. (C) Whole-cell extracts were separated by SDS-PAGE, and in-gel kinase assays were carried out with MBP embedded in the gel as the kinase substrate. The disruption of the actin cytoskeleton increased MBP phosphorylation at a position coincident with MST1 and MST2 mass (P-MBP). The positions of molecular size markers are indicated. The quantification of ^{32}P incorporation revealed that the increase (n-fold) in kinase activity relative to that of untreated cells was significantly increased in CTD- and Tat-C3-treated cells (**, $P < 0.01$; *, $P < 0.05$; both by Student's t test; data are means ± standard errors of the means; $n = 6$).

structures with CTD induced significantly increased phosphorylation of endogenous c-Jun, as determined by the quantitative direct scanning of Western blots and near-infrared fluorophore-conjugated secondary antibodies, which could be significantly reduced by the coadministration of the JNK inhibitor SP600125 (Fig. 3A) (5). The expression of FLAG-tagged MST1 or MST2 also induced significantly increased levels of c-Jun phosphorylation, which also were significantly reduced by the JNK inhibitor SP600125 (Fig. 3A). The expression of MST1 or MST2 elevated in-gel MBP kinase activity at the same molecular weight as that of the endogenous activity, while kinase-dead MST2 was able to inhibit basal MST kinase activity (Fig. 3B). JNK1 was immunoprecipitated and assayed for in vitro kinase activity using recombinant GST–c-Jun (amino acids 1 to 79) as the substrate, which revealed that JNK1 activity was induced by ectopically expressed MST1 or MST2 (Fig. 3C). JNK1 activity was elevated following Tat-C3 treatment, which was reduced by the expression of dominant-negative MST2 (Fig. 3D). Consistently with this observation, JNK1 activity was elevated following actin disruption by LTB, CTD, or Tat-C3 treatment, which again was significantly reduced by dominant-negative MST2 (Fig. 3E). Finally, the significant 50% reduction in MST2 expression by siRNA-mediated knockdown was paralleled by a significant 50% reduction in CTD-induced c-Jun phosphorylation (Fig. 3F). These results indicate that the disruption of the actin cytoskeleton activates MST, which leads to MST-dependent JNK activation and substrate phosphorylation.

Stabilization of p21 by MST and JNK in response to actin disruption. We previously showed that the disruption of actin structures and consequent JNK activation stabilized the CDKI p21 using radioactive pulse-chase assays (14). These findings were confirmed in assays using the protein translation inhibitor emetine to block new synthesis (28) and in comparisons to p21 levels in untreated cells. After 2 h of emetine treatment, FLAG-tagged p21 protein levels were reduced by ~50% compared to those of the control while ERK2 levels were unchanged, indicating that p21 protein was relatively unstable (Fig. 4A and B). The inactivation of RhoA by Tat-C3 produced a characteristic shift in mobility due to ADP-ribosylation, and, consistently with previous results (14), it stabilized p21, which was reflected by the increased protein level remaining after emetine treatment (Fig. 4A and B). Actin disruption with CTD or TAT-C3 significantly increased the amount of p21 remaining in the emetine treatment group (Fig. 4B). In addition to actin disruption, p21 stabilization could be induced by the expression of MST2 or MST1 (Fig. 4C). Consistently with our previous finding that the stabilization of p21 following actin disruption was dependent upon the JNK pathway (14), the JNK inhibitor SP600125 (5) significantly reduced MST2-induced p21 stabilization (Fig. 4D). The ability of Tat-C3 to stabilize p21 could be reversed by the expression of kinase-dead MST2 (Fig. 4E) that also had inhibited Tat-C3-induced JNK activation (Fig. 3C). Taken together, these data indicate that the stabilization of p21 following actin cytoskeletal disruption results from the MST-mediated activation of the JNK pathway.

The stability of p21 is influenced by phosphorylation (12), although the effects of phosphorylation at specific sites may vary under different conditions and in different cell types. We examined how candidate phosphorylation sites contributed to

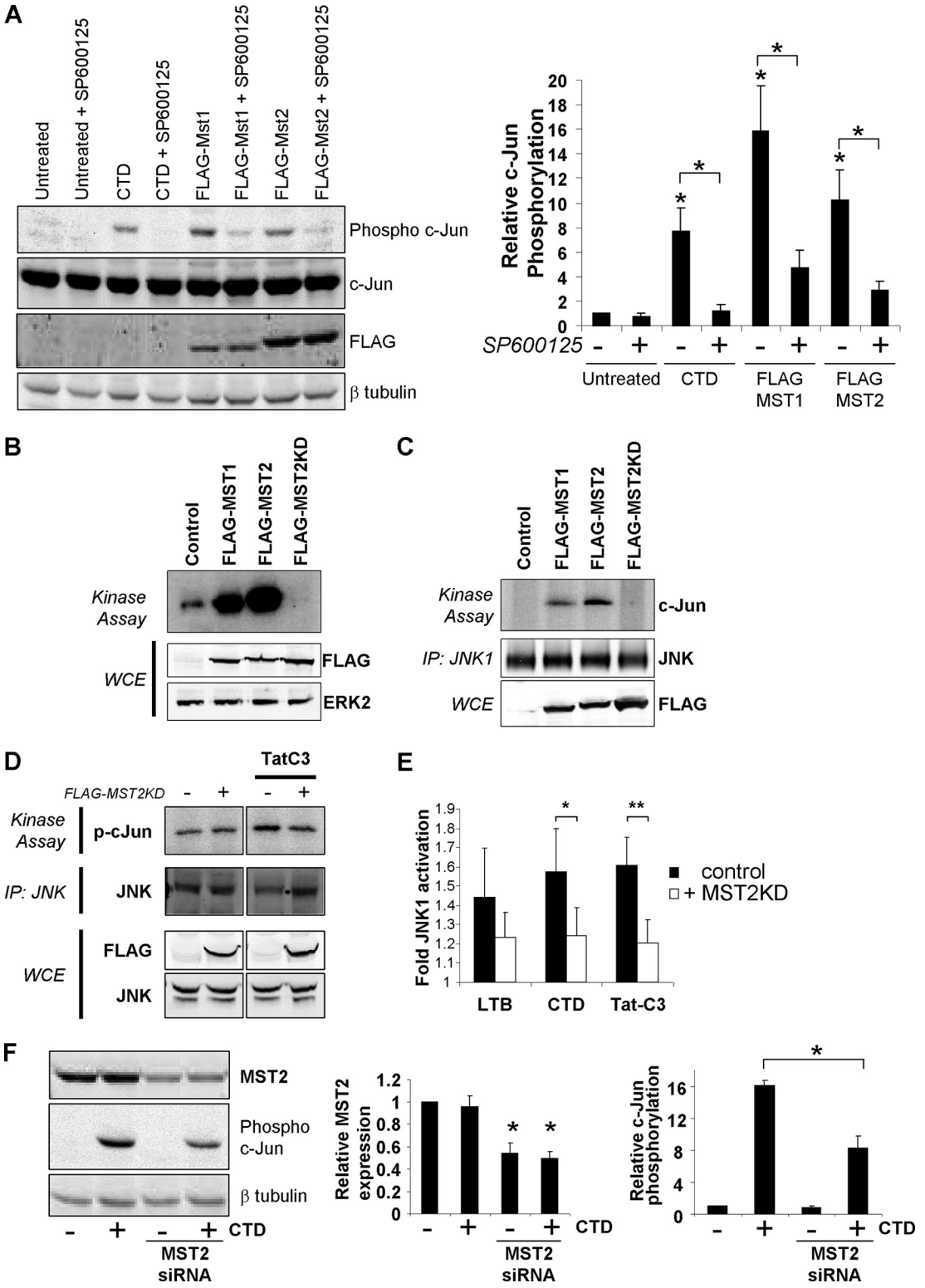

FIG. 3. JNK activation by actin disruption via MST. (A) Activation of JNK and sensitivity to JNK inhibitor SP600125 were determined by Western blotting for c-Jun phosphorylation (left). The ratios of phospho-c-Jun/total c-Jun relative to those of untreated cells are shown in right panel. Treatment with CTD significantly induced c-Jun phosphorylation that could be significantly reduced by SP600125, similarly to the effects of MST1 or MST2 expression. (*, $P < 0.05$ by Student's t test compared to results for untreated cells or cells treated with SP600125 as indicated; data are means ± standard errors of the means; $n = 3$). (B) Expression of FLAG-MST1 or FLAG-MST2 increased MBP kinase activity above basal levels, while a kinase-dead version of MST2 (MST2KD) inhibited basal kinase activity, indicating that it acts in a dominant-negative manner. WCE, whole-cell extract. (C) Expression of FLAG-MST1 or FLAG-MST2 increased endogenous JNK1 kinase activity. JNK1 was immunoprecipitated (IP) from transfected cells and assayed for the phosphorylation of recombinant c-Jun in vitro. (D) Dominant-negative kinase-dead MST2 (MST2KD) inhibited JNK1 kinase activity induced by TatC3. (E) Dominant-negative kinase-dead MST2 (MST2KD) inhibited JNK1 kinase activity induced by actin cytoskeleton disruption (**, $P < 0.01$; *, $P < 0.05$; both by Student's t test; data are means ± standard errors of the means; $n = 13$). (F) Knockdown of MST2 by siRNA significantly reduced the CTD-induced c-Jun phosphorylation (*, $P < 0.01$ by Student's t test; data are means ± standard errors of the means; $n = 3$).

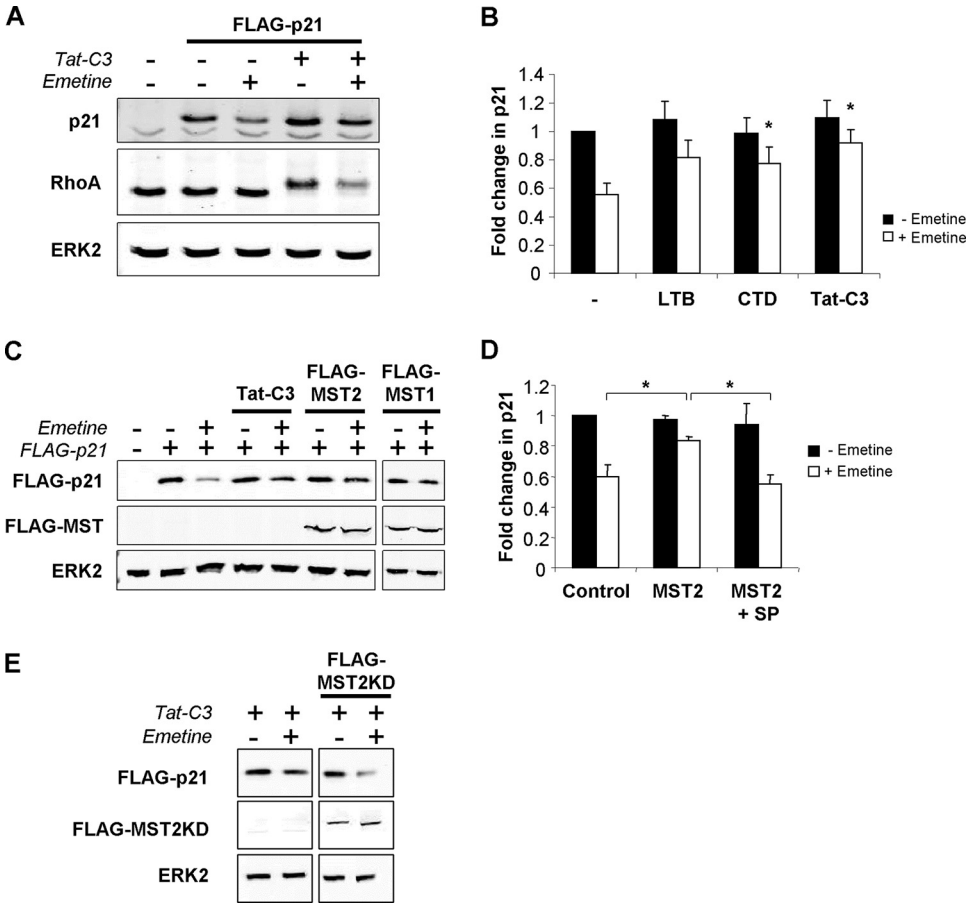

FIG. 4. Turnover of p21 is inhibited by MST activation of the JNK pathway. (A) Inhibition of protein translation with emetine for 2 h revealed that FLAG-p21 levels decreased while RhoA and ERK2 levels remained constant, indicating that p21 is relatively unstable. The inhibition of RhoA with Tat-C3 maintained p21 levels remaining after emetine treatment, indicating increased protein stability. (B) Disruption of the actin cytoskeleton increased the proportion of p21 remaining after emetine treatment, which is indicative of increased protein stability (*, $P < 0.05$ by Student's t test; data are means ± standard errors of the means; $n = 6$). (C) Increased levels of p21 following 2 h of emetine treatment in cells expressing FLAG-tagged MST1 or MST2, which is indicative of increased p21 stability. (D) The increased p21 stability induced by MST2 expression could be reversed by the JNK inhibitor SP600125 (SP; 30 μM) (*, $P < 0.05$ by Student's t test; data are means ± standard errors of the means; $n = 4$). (E) Stabilization of p21 induced by Tat-C3 can be reversed by kinase-dead MST2.

Tat-C3-induced stabilization by mutating each to nonphosphorylatable alanine residues. Threonine 57 (T57) (35), serine 98 (S98) (57), and serine 130 (S130) (35) each have been shown to be phosphorylated by JNK, and in the case of T57 and S130 these phosphorylations were reported to affect p21 stability (35). Phosphorylation on threonine 145 (T145) and serine 146 (S146) also may affect p21 protein stability; however, both increased and decreased stabilization have been reported (12). We analyzed the stability of the wild type and point mutants with or without Tat-C3 treatment. As before, Tat-C3 treatment resulted in p21 stabilization (Fig. 5A, upper left). In contrast, the stability of a T57A mutant was comparable with or without Tat-C3 treatment (Fig. 5A, upper middle), indicating that this site likely contributed to p21 stabilization in response to actin disruption. The S98A (Fig. 5A, upper right) and T145A (Fig. 5A, lower middle) mutants responded similarly to wild-type p21, indicating that they did not contribute to p21 stabilization. S130A (Fig. 5A, lower left) and S146A (Fig. 5A, lower right) were more stable than wild-type p21, suggesting that these sites contribute to basal protein turnover (48), but they were unlikely to contribute to stabilization in response to actin disruption.

We previously found that the direct activation of the JNK pathway with the active MAP3K MEKK1 was sufficient to stabilize p21 in radioactive pulse-chase assays (14). Using the emetine translation inhibition assay, we found that MEKK1 increased p21 stability comparably to that by Tat-C3 (Fig. 5B). In marked contrast, the T57A p21 mutant no longer was stabilized by Tat-C3 or MEKK1 (Fig. 5C). Finally, the ability of MST1 or MST2 to stabilize p21 (Fig. 4B) was markedly reduced in the T57A mutant (Fig. 5D). These results indicate that the T57 site mediates the JNK-induced stabilization of p21 that results from the activation of this SAPK pathway either directly or in response to actin disruption via MST kinases.

The ability of JNK to phosphorylate p21 on T57 (35) is associated with a direct interaction between these proteins (49, 55). We wished to determine whether the disruption of the actin cytoskeleton would affect the association of JNK with p21. When FLAG-tagged p21 was immunoprecipitated from cells that were left untreated or were treated with Tat-C3,

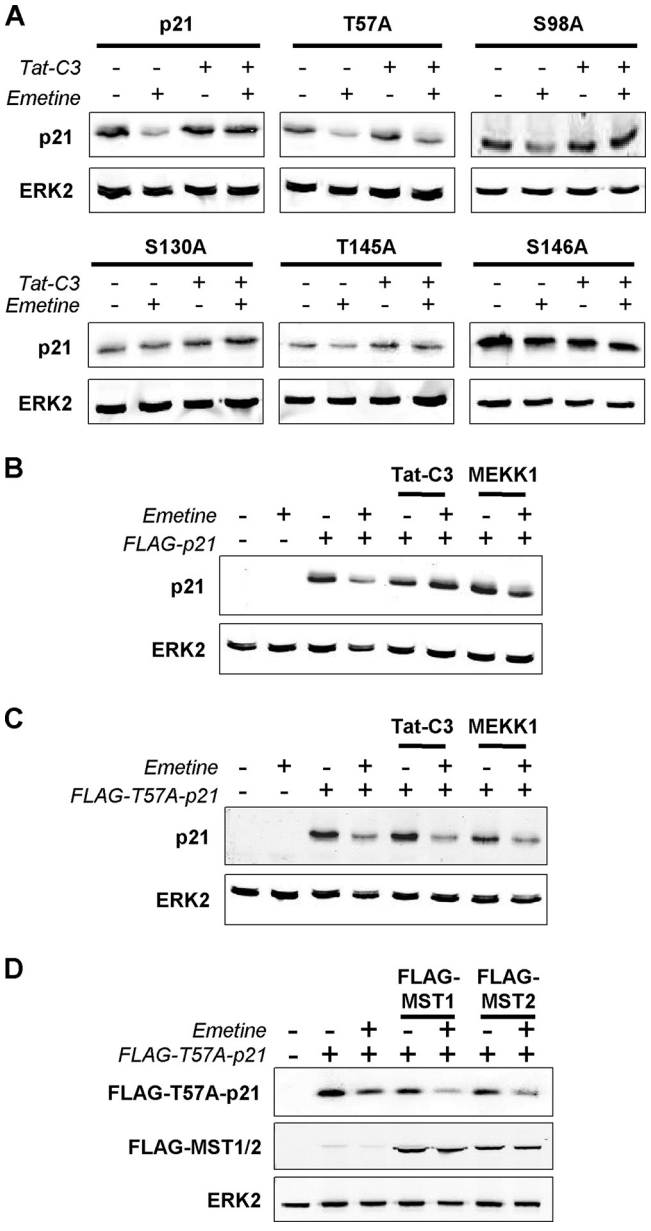

FIG. 5. Thr57 is required for p21 stabilization by actin disruption, MST kinases, or JNK. (A) Phosphorylation sites reported to regulate p21 stability were mutated individually to nonphosphorylatable alanine residues. Mutants were expressed and protein levels determined following treatment with or without Tat-C3 and the protein synthesis inhibitor emetine as indicated. While Tat-C3 elevated levels of wild-type p21 in emetine-treated cells, indicating increased protein stability, the nonphosphorylatable T57A mutant was not stabilized in response to Tat-C3. S98A and T145A mutants were stabilized by Tat-C3 compared to the stabilization of untreated cells, while the S130A and S146A mutants appeared to increase basal stability. Therefore, T57 appeared to be the critical site for stabilization in response to Tat-C3. (B) Stabilization of p21 by Tat-C3 or direct activation of the JNK pathway by the MAP3K MEKK1. (C) Stabilization of p21 by Tat-C3 or MEKK1 was reduced in the T57A p21 mutant. (D) The p21 T57A mutant no longer was stabilized by MST1 or MST2.

there was no marked difference in the amount of endogenous JNK1 and JNK2 that was associated (Fig. 6A). The ability of recombinant JNK1 to phosphorylate p21 in vitro was lost when T57 was mutated to a nonphosphorylatable alanine (Fig. 6B), indicating that this site likely is the major JNK phosphorylation site. Although it is consistent with previous studies showing that p21 is a bona fide JNK substrate (49), p21 phosphorylation appeared to be less efficient than that for recombinant c-Jun (Fig. 6B, right). These data indicate that the activation of JNK following actin disruption does not affect the association between JNK and p21 but promotes p21 protein stabilization via phosphorylation on T57.

DISCUSSION

As well as providing a structural framework, the actin cytoskeleton plays integral roles in cell death, survival, and proliferation. One way that information about the mechanical stresses that produce strain on the cytoskeleton, or even result in cytoskeletal disintegration, may be transmitted is via the SAPK pathways. The ultimate cellular response to SAPK signaling induced by alterations to the actin cytoskeleton depends on a number of variables, including signal intensity and duration, cell type, and context. The mechanisms that sense the status of actin structures and couple to SAPK pathways have not been characterized in mammalian cells. In this study, we report that MST kinases are activated in response to the disruption of the actin cytoskeleton, which in turns leads to the activation of the JNK SAPK (Fig. 7). One effect of MST-JNK activation following actin disruption is the JNK-mediated phosphorylation and consequent stabilization of the CDKI p21. These data reveal the mechanism that links the sensing of cytoskeletal integrity to a key cell cycle regulatory protein.

An intact actin cytoskeleton and normal Rho signaling are required for cell proliferation, whereas Rho inhibition and the loss of cytoskeletal integrity are associated with cell cycle arrest (9, 32, 40, 41, 44, 46). In addition, the arrest of adherent cells placed in suspension has been associated with actin disruption and high p21 levels (10, 25, 58). These findings have prompted the development of inhibitors that are able to block Rho function by targeting critical posttranslational modifications as antiproliferative agents (54). One way this has been achieved is to block geranylgeranyl transferase I (GGTase I), which catalyzes the attachment of a 20-carbon geranylgeranyl group to the cysteine in the carboxyl-terminal CAAX box. GGTase inhibitors efficiently block RhoA modification and lead to p21-mediated cell cycle arrest (1). An alternative strategy is to inhibit 3-hydroxy-3-methylglutaryl (HMG)–coenzyme A (CoA) reductase, which limits geranylgeranyl pyrophosphate production by inhibiting the conversion of HMG-CoA to mevalonate (a five-carbon molecule required for geranylgeranyl pyrophosphate synthesis), resulting in cell cycle arrest associated with RhoA inactivation and increased p21 levels (18–20). Following geranylgeranylation, the Rce1 endopeptidase removes the terminal three amino acids from the RhoA CAAX box, and finally the isoprenylated cysteine is methylated by the isoprenylcysteine carboxyl methyltransferase (ICMT). The genetic inactivation of ICMT inhibited K-Ras- and B-Raf-mediated fibroblast transformation by lowering RhoA protein levels and consequently elevating p21 (6). The physiological inactivation of RhoA can be induced in smooth-muscle cells by nitric oxide, resulting in p21 elevation and the inhibition of proliferation (59). These results reinforce the strong requirement for Rho

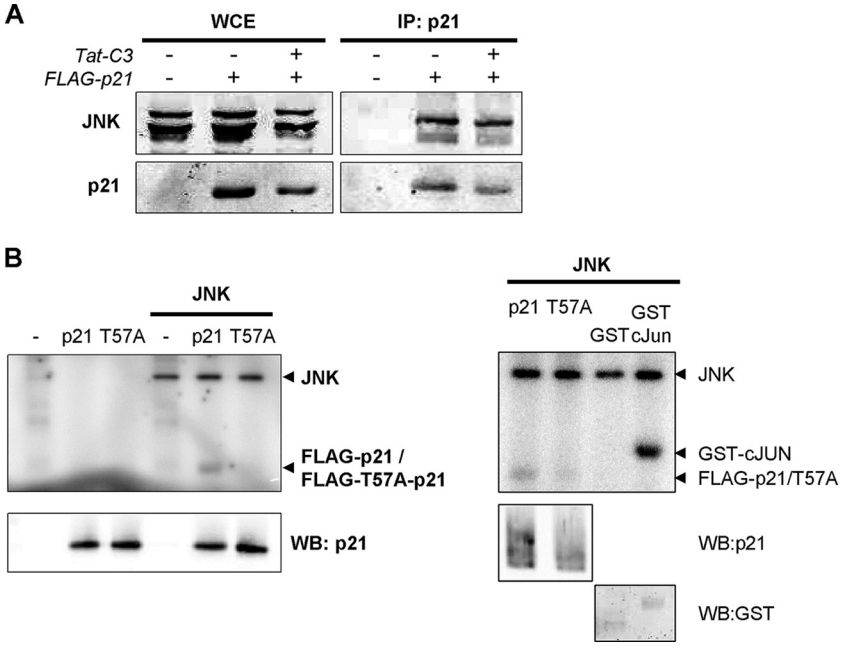

FIG. 6. Association of JNK with p21 and phosphorylation on Thr57. (A) Immunoprecipitated (IP) FLAG-tagged p21 copurifies with endogenous JNK kinases. Treatment with Tat-C3 did not affect the levels of copurified JNK protein. WCE, whole-cell extract. (B) The ability of recombinant JNK1 to phosphorylate p21 was greatly reduced by the mutation of T57 to alanine. WB, Western blotting.

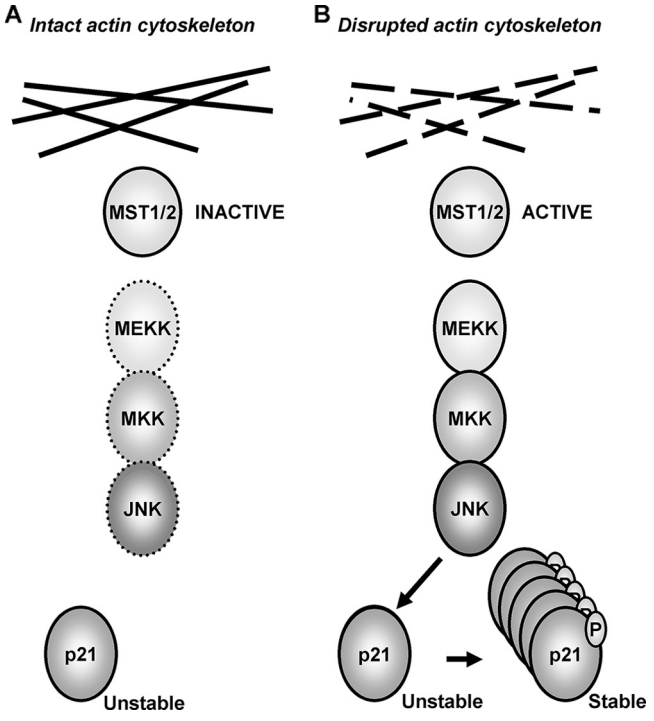

FIG. 7. Model of role played by MST kinases linking the integrity of the actin cytoskeleton via the JNK SAPK pathway to the phosphorylation and stability of p21. (A) Under conditions of actin cytoskeletal integrity, MST kinases have low activity and do not significantly activate the JNK SAPK pathway. As a consequence, p21 is not phosphorylated on Thr57 and is relatively unstable. (B) Following the disruption of cytoskeletal integrity, MST becomes activated, leading to increased JNK SAPK activity and increased p21 phosphorylation on Thr57, resulting in protein stabilization.

activity to restrict p21 levels to permit cell cycle progression and proliferation.

We and others have demonstrated previously that Rho influences p21 levels at least in part by transcriptional mechanisms (1, 30, 38, 41). There also are posttranscriptional mechanisms by which the disruption of the actin cytoskeleton increases p21 levels. Agents that act directly on actin filaments, or indirectly via Rho inhibition, induce cell cycle arrest associated with the reduced phosphorylation of the retinoblastoma protein by stabilizing p21 protein, which leads to its accumulation (14, 37). The p21 stabilization results from the activation of JNK in response to the loss of cytoskeletal integrity (14). The mechanisms linking the monitoring of cytoskeletal integrity to JNK activation previously were unknown; we now show that the connection between the disruption of the actin cytoskeleton and the consequent JNK activation that leads to p21 stabilization is mediated by MST kinases.

Saccharomyces cerevisiae provides a useful template for studying the connection between the actin cytoskeleton and the regulation of cell cycle progression. The disruption of actin structures activates Ssk2p, which lies upstream of the Hog1 SAPK (7). In turn, Hog1 phosphorylates and stabilizes the CDKI Sic1 and inhibits the CDK Cdc28 (24). In this study, we found that cytoskeletal disruption activates MST, which lies upstream of the JNK SAPK pathway. The CDKI p21 is stabilized by JNK-mediated phosphorylation following actin disruption. Although the individual components are not homologues (e.g., MST $\neq$ Ssk2p and p21 $\neq$ Sic1), there is a striking similarity in the way that actin disruption activates SAPK signaling, leading to the phosphorylation and stabilization of a CDKI and suggesting that the two pathways are analogous. One possibility is that the larger number of proteins in higher eukaryotes that play similar roles (e.g., multiple MAP4K proteins and

CDKIs) has allowed for plasticity in the identities of the individual components that contribute to a functionally analogous mechanism. Alternatively, this may be an example of convergent evolution in which a similar stimulus-response relationship has been selected for but that use different components to achieve comparable endpoints. The recurrence of cell cycle checkpoints that monitor the actin cytoskeleton highlights the importance of restricting cell proliferation to the correct environmental context. The loss of these checkpoints may permit anchorage-independent cell proliferation, a hallmark of cancer.

Although MST kinases were identified because of their possible function as MAP4K that regulate SAPK pathways (17), much recent interest has been focused on the *Drosophila melanogaster* orthologue Hippo, which is a key regulator of cell growth, proliferation, and survival (31). In this signaling pathway, Hippo associates with the Salvador scaffold protein and phosphorylates and activates the NDR kinase warts, which is homologous to the mammalian Lats tumor suppressors. The activity of *hippo* is influenced by the F-actin binding proteins merlin and expanded, which can act as cytoskeletal anchors. However, the *hippo*-MST in the *salvador-warts-hippo* signaling network may be completely independent of MST acting upstream of SAPK regulation in response to cytoskeletal disruption. There are examples of kinases acting in distinct signaling pathways by being physically distributed in discrete protein complexes and insulated from potential cross-talk. A case in point is glycogen synthase kinase 3-β, which acts downstream of the insulin receptor to regulate glycogen synthase activity and downstream of Wnt to regulate β-catenin stability (13). The stimulation of cells with insulin does not result in the stabilization of β-catenin, because signaling is restricted to the pool of glycogen synthase kinase 3-β not associated with the multiprotein complex that acts in response to Wnt (22). In this manner, the same kinase can be dedicated to distinct signaling pathways and therefore evoke independent downstream responses. That said, it is interesting that in the context of the *salvador-warts-hippo* signaling complex, *hippo* represses cyclin E transcription, while following F-actin disruption MST stabilizes p21, indicating that there is a recurring role of *hippo*-MST as a negative cell cycle regulator independently of its mode of activation.

Active JNK has been found in association with F-actin (29), where it may contribute to regulating actin polymerization and remodelling (4). Although in *Saccharomyces cerevisiae* the MAP3K Ssk2p contributes to actin recovery following osmotic stress, this process is not mediated via the Hog1 SAPK pathway but instead results from the association of Ssk2p with the polarisome complex and the formin protein Bni1p to mediate polarized actin polymerization (8). Using matrix-assisted laser desorption ionization–time of flight mass spectrometry, we identified β-actin as a copurified protein with MST2; however, purified β-actin did not associate with recombinant MST2 in vitro (data not shown), suggesting that any interactions between MST2 and F-actin are indirect. We did not observe changes in actin organization in cells expressing MST1 or MST2 despite the fact that JNK1 was activated, suggesting that elevated MST-JNK signaling is not sufficient to affect the actin cytoskeleton in basal conditions. However, it remains to be determined whether the MST-mediated activation of JNK contributes to actin recovery. A role for MST in a JNK-independent actin recovery complex that employs formin proteins to catalyze actin polymerization is possible but seems unlikely, given that the LD domain of Ssk2p that is critical for actin recovery is not present in MST (8).

ACKNOWLEDGMENTS

This research was supported by Cancer Research UK and a grant to M.F.O. from the NIH (CA030721).

REFERENCES

1. **Adnane, J., F. A. Bizouarn, Y. Qian, A. D. Hamilton, and S. M. Sebti.** 1998. $p21^{WAF1/CIP1}$ is upregulated by the geranylgeranyltransferase I inhibitor GGTI-298 through a transforming growth factor beta- and Sp1-responsive element: involvement of the small GTPase *rhoA*. Mol. Cell. Biol. **18:**6962–6970.
2. **Ailenberg, M., and M. Silverman.** 2003. Cytochalasin D disruption of actin filaments in 3T3 cells produces an anti-apoptotic response by activating gelatinase A extracellularly and initiating intracellular survival signals. Biochim. Biophys. Acta **1593:**249–258.
3. **Aktories, K., C. Mohr, and G. Koch.** 1992. Clostridium botulinum C3 ADP-ribosyltransferase. Curr. Top. Microbiol. Immunol. **175:**115–131.
4. **Altan, Z. M., and G. Fenteany.** 2004. c-Jun N-terminal kinase regulates lamellipodial protrusion and cell sheet migration during epithelial wound closure by a gene expression-independent mechanism. Biochem. Biophys. Res. Commun. **322:**56–67.
5. **Bennett, B. L., D. T. Sasaki, B. W. Murray, E. C. O'Leary, S. T. Sakata, W. Xu, J. C. Leisten, A. Motiwala, S. Pierce, Y. Satoh, S. S. Bhagwat, A. M. Manning, and D. W. Anderson.** 2001. SP600125, an anthrapyrazolone inhibitor of Jun N-terminal kinase. Proc. Natl. Acad. Sci. USA **98:**13681–13686.
6. **Bergo, M. O., B. J. Gavino, C. Hong, A. P. Beigneux, M. McMahon, P. J. Casey, and S. G. Young.** 2004. Inactivation of Icmt inhibits transformation by oncogenic K-Ras and B-Raf. J. Clin. Investig. **113:**539–550.
7. **Bettinger, B. T., and D. C. Amberg.** 2007. The MEK kinases MEKK4/Ssk2p facilitate complexity in the stress signaling responses of diverse systems. J. Cell Biochem. **101:**34–43.
8. **Bettinger, B. T., M. G. Clark, and D. C. Amberg.** 2007. Requirement for the polarisome and formin function in Ssk2p-mediated actin recovery from oSmotic stress in Saccharomyces cerevisiae. Genetics **175:**1637–1648.
9. **Böhmer, R. M., E. Scharf, and R. K. Assoian.** 1996. Cytoskeletal integrity is required throughout the mitogen stimulation phase of the cell cycle and mediates the anchorage-dependent expression of cyclin D1. Mol. Biol. Cell **7:**101–111.
10. **Bottazzi, M. E., X. Zhu, R. M. Bohmer, and R. K. Assoian.** 1999. Regulation of $p21^{cip1}$ expression by growth factors and the extracellular matrix reveals a role for transient ERK activity in G1 phase. J. Cell Biol. **146:**1255–1264.
11. **Cherng, Y. G., H. C. Chang, Y. L. Lin, M. L. Kuo, W. T. Chiu, and R. M. Chen.** 2008. Apoptotic insults to human chondrocytes induced by sodium nitroprusside are involved in sequential events, including cytoskeletal remodeling, phosphorylation of mitogen-activated protein kinase kinase kinase-1/c-Jun N-terminal kinase, and Bax-mitochondria-mediated caspase activation. J. Orthop. Res. **26:**1018–1026.
12. **Child, E. S., and D. J. Mann.** 2006. The intricacies of p21 phosphorylation: protein/protein interactions, subcellular localization and stability. Cell Cycle **5:**1313–1319.
13. **Cohen, P., and S. Frame.** 2001. The renaissance of GSK3. Nat. Rev. Mol. Cell Biol. **2:**769–776.
14. **Coleman, M. L., R. M. Densham, D. R. Croft, and M. F. Olson.** 2006. Stability of $p21^{Waf1/Cip1}$ CDK inhibitor protein is responsive to RhoA-mediated regulation of the actin cytoskeleton. Oncogene **25:**2708–2716.
15. **Coleman, M. L., C. J. Marshall, and M. F. Olson.** 2003. Ras promotes $p21^{Waf1/Cip1}$ protein stability via a cyclin D1-imposed block in proteasome-mediated degradation. EMBO J. **22:**2036–2046.
16. **Coleman, M. L., E. A. Sahai, M. Yeo, M. Bosch, A. Dewar, and M. F. Olson.** 2001. Membrane blebbing during apoptosis results from caspase-mediated activation of ROCK I. Nat. Cell Biol. **3:**339–345.
17. **Creasy, C. L., and J. Chernoff.** 1995. Cloning and characterization of a human protein kinase with homology to Ste20. J. Biol. Chem. **270:**21695–21700.
18. **Danesh, F. R., M. M. Sadeghi, N. Amro, C. Philips, L. Zeng, S. Lin, A. Sahai, and Y. S. Kanwar.** 2002. 3-Hydroxy-3-methylglutaryl CoA reductase inhibitors prevent high glucose-induced proliferation of mesangial cells via modulation of Rho GTPase/ p21 signaling pathway: implications for diabetic nephropathy. Proc. Natl. Acad. Sci. USA **99:**8301–8305.
19. **Denoyelle, C., P. Albanese, G. Uzan, L. Hong, J. P. Vannier, J. Soria, and C. Soria.** 2003. Molecular mechanism of the anti-cancer activity of cerivastatin, an inhibitor of HMG-CoA reductase, on aggressive human breast cancer cells. Cell Signal. **15:**327–338.
20. **Denoyelle, C., M. Vasse, M. Korner, Z. Mishal, F. Ganne, J. P. Vannier, J. Soria, and C. Soria.** 2001. Cerivastatin, an inhibitor of HMG-CoA reductase,

inhibits the signaling pathways involved in the invasiveness and metastatic properties of highly invasive breast cancer cell lines: an in vitro study. Carcinogenesis **22:**1139–1148.
21. **Diez, S., G. Gerisch, K. Anderson, A. Muller-Taubenberger, and T. Bretschneider.** 2005. Subsecond reorganization of the actin network in cell motility and chemotaxis. Proc. Natl. Acad. Sci. USA **102:**7601–7606.
22. **Ding, V. W., R. H. Chen, and F. McCormick.** 2000. Differential regulation of glycogen synthase kinase 3β by insulin and Wnt signaling. J. Biol. Chem. **275:**32475–32481.
23. **Dunn, C., C. Wiltshire, A. MacLaren, and D. A. Gillespie.** 2002. Molecular mechanism and biological functions of c-Jun N-terminal kinase signalling via the c-Jun transcription factor. Cell Signal. **14:**585–593.
24. **Escoté, X., M. Zapater, J. Clotet, and F. Posas.** 2004. Hog1 mediates cell-cycle arrest in G1 phase by the dual targeting of Sic1. Nat. Cell Biol. **6:**997–1002.
25. **Fang, F., G. Orend, N. Watanabe, T. Hunter, and E. Ruoslahti.** 1996. Dependence of cyclin E-CDK2 kinase activity on cell anchorage. Science **271:** 499–502.
26. **Graves, J. D., K. E. Draves, Y. Gotoh, E. G. Krebs, and E. A. Clark.** 2001. Both phosphorylation and caspase-mediated cleavage contribute to regulation of the Ste20-like protein kinase MstI during CD95/Fas-induced apoptosis. J. Biol. Chem. **276:**14909–14915.
27. **Graves, J. D., Y. Gotoh, K. E. Draves, D. Ambrose, D. K. Han, M. Wright, J. Chernoff, E. A. Clark, and E. G. Krebs.** 1998. Caspase-mediated activation and induction of apoptosis by the mammalian Ste20-like kinase MstI. EMBO J. **17:**2224–2234.
28. **Grollman, A. P.** 1966. Structural basis for inhibition of protein synthesis by emetine and cycloheximide based on an analogy between ipecac alkaloids and glutarimide antibiotics. Proc. Natl. Acad. Sci. USA **56:**1867–1874.
29. **Hamel, M., D. Kanyi, M. D. Cipolle, and L. Lowe-Krentz.** 2006. Active stress kinases in proliferating endothelial cells associated with cytoskeletal structures. Endothelium **13:**157–170.
30. **Han, S., N. Sidell, and J. Roman.** 2005. Fibronectin stimulates human lung carcinoma cell proliferation by suppressing p21 gene expression via signals involving Erk and Rho kinase. Cancer Lett. **219:**71–81.
31. **Harvey, K., and N. Tapon.** 2007. The Salvador-Warts-Hippo pathway—an emerging tumour-suppressor network. Nat. Rev. Cancer **7:**182–191.
32. **Huang, S., and D. E. Ingber.** 2002. A discrete cell cycle checkpoint in late G_1 that is cytoskeleton-dependent and MAP kinase (Erk)-independent. Exp. Cell Res. **275:**255–264.
33. **Jaffe, A. B., and A. Hall.** 2005. Rho GTPases: biochemistry and biology. Annu. Rev. Cell Dev. Biol. **21:**247–269.
34. **Kaunas, R., S. Usami, and S. Chien.** 2006. Regulation of stretch-induced JNK activation by stress fiber orientation. Cell Signal. **18:**1924–1931.
35. **Kim, G. Y., S. E. Mercer, D. Z. Ewton, Z. Yan, K. Jin, and E. Friedman.** 2002. The stress-activated protein kinases p38α and JNK1 stabilize p21Cip1 by phosphorylation. J. Biol. Chem. **277:**29792–29802.
36. **Lee, K.-K., and S. Yonehara.** 2002. Phosphorylation and dimerization regulate nucleocytoplasmic shuttling of mammalian STE20-like kinase (MST). J. Biol. Chem. **277:**12351–12358.
37. **Lee, Y. J., C. H. Tsai, J. J. Hwang, S. J. Chiu, T. J. Sheu, and P. C. Keng.** 2009. Involvement of a p53-independent and post-transcriptional up-regulation for p21WAF/CIP1 following destabilization of the actin cytoskeleton. Int. J. Oncol. **34:**581–589.
38. **Liberto, M., D. Cobrinik, and A. Minden.** 2002. Rho regulates p21(CIP1), cyclin D1, and checkpoint control in mammary epithelial cells. Oncogene **21:**1590–1599.
39. **Matallanas, D., D. Romano, K. Yee, K. Meissl, L. Kucerova, D. Piazzolla, M. Baccarini, J. K. Vass, W. Kolch, and E. O'Neill.** 2007. RASSF1A elicits apoptosis through an MST2 pathway directing proapoptotic transcription by the p73 tumor suppressor protein. Mol. Cell **27:**962–975.
40. **Olson, M. F., A. Ashworth, and A. Hall.** 1995. An essential role for Rho, Rac, and Cdc42 GTPases in cell cycle progression through G1. Science **269:**1270–1272.
41. **Olson, M. F., H. F. Paterson, and C. J. Marshall.** 1998. Signals from Ras and Rho GTPases interact to regulate expression of p21Waf1/Cip1. Nature **394:** 295–299.
42. **O'Neill, E., L. Rushworth, M. Baccarini, and W. Kolch.** 2004. Role of the kinase MST2 in suppression of apoptosis by the proto-oncogene product Raf-1. Science **306:**2267–2270.
43. **Raman, M., W. Chen, and M. H. Cobb.** 2007. Differential regulation and properties of MAPKs. Oncogene **26:**3100–3112.
44. **Reshetnikova, G., R. Barkan, B. Popov, N. Nikolsky, and L. S. Chang.** 2000. Disruption of the actin cytoskeleton leads to inhibition of mitogen-induced cyclin E expression, Cdk2 phosphorylation, and nuclear accumulation of the retinoblastoma protein-related p107 protein. Exp. Cell Res. **259:**35–53.
45. **Sahai, E., and M. F. Olson.** 2006. Purification of TAT-C3 exoenzyme. Methods Enzymol. **406:**128–140.
46. **Sahai, E., M. F. Olson, and C. J. Marshall.** 2001. Cross-talk between Ras and Rho signalling pathways in transformation favours proliferation and increased motility. EMBO J. **20:**755–766.
47. **Sampath, P., and T. D. Pollard.** 1991. Effects of cytochalasin, phalloidin, and pH on the elongation of actin filaments. Biochemistry **30:**1973–1980.
48. **Scott, M. T., A. Ingram, and K. L. Ball.** 2002. PDK1-dependent activation of atypical PKC leads to degradation of the p21 tumour modifier protein. EMBO J. **21:**6771–6780.
49. **Shim, J., H. Lee, J. Park, H. Kim, and E. J. Choi.** 1996. A non-enzymatic p21 protein inhibitor of stress-activated protein kinases. Nature **381:**804–806.
50. **Spector, I., N. R. Shochet, Y. Kashman, and A. Groweiss.** 1983. Latrunculins: novel marine toxins that disrupt microfilament organization in cultured cells. Science **219:**493–495.
51. **Strange, K., J. Denton, and K. Nehrke.** 2006. Ste20-type kinases: evolutionarily conserved regulators of ion transport and cell volume. Physiology **21:** 61–68.
52. **Taylor, L. K., H.-C. R. Wang, and R. L. Erikson.** 1996. Newly identified stress-responsive protein kinases, Krs-1 and Krs-2. Proc. Natl. Acad. Sci. USA **93:**10099–10104.
53. **Ura, S., H. Nishina, Y. Gotoh, and T. Katada.** 2007. Activation of the c-Jun N-terminal kinase pathway by MST1 Is essential and sufficient for the induction of chromatin condensation during apoptosis. Mol. Cell. Biol. **27:** 5514–5522.
54. **Walker, K., and M. F. Olson.** 2005. Targeting Ras and Rho GTPases as opportunities for cancer therapeutics. Curr. Opin. Genet. Dev. **15:**62–68.
55. **Yue, X., T. R. Nadja, H. Xiaoman, and C. P. Jill.** 2003. Association of JNK1 with p21waf1 and p53: modulation of JNK1 activity. Mol. Carcinogenesis **36:**38–44.
56. **Yuzyuk, T., M. Foehr, and D. C. Amberg.** 2002. The MEK kinase Ssk2p promotes actin cytoskeleton recovery after osmotic stress. Mol. Biol. Cell **13:**2869–2880.
57. **Zhan, J., J. B. Easton, S. Huang, A. Mishra, L. Xiao, E. R. Lacy, R. W. Kriwacki, and P. J. Houghton.** 2007. Negative regulation of ASK1 by p21Cip1 involves a small domain that includes serine 98 that is phosphorylated by ASK1 in vivo. Mol. Cell. Biol. **27:**3530–3541.
58. **Zhu, X., M. Ohtsubo, R. M. Bohmer, J. M. Roberts, and R. K. Assoian.** 1996. Adhesion-dependent cell cycle progression linked to the expression of cyclin D1, activation of cyclin E-cdk2, and phosphorylation of the retinoblastoma protein. J. Cell Biol. **133:**391–403.
59. **Zuckerbraun, B. S., D. A. Stoyanovsky, R. Sengupta, R. A. Shapiro, B. A. Ozanich, J. Rao, J. E. Barbato, and E. Tzeng.** 2007. Nitric oxide-induced inhibition of smooth muscle cell proliferation involves S-nitrosation and inactivation of RhoA. Am. J. Physiol. Cell Physiol. **292:**C824–C831.